J. Fluid Mech. (2008), *vol.* 601, *pp.* 165–187.
doi:10.1017/S0022112008000669 Printed in the United Kingdom

Receptivity of a hypersonic boundary layer over a flat plate with a porous coating

I. V. EGOROV, A. V. FEDOROV AND V. G. SOUDAKOV

Department of Aeromechanics and Flight Engineering, Moscow Institute of Physics and Technology, Zhukovsky, 140180, Russia

(Received 19 June 2006 and in revised form 25 December 2007)

Two-dimensional direct numerical simulation (DNS) of receptivity to acoustic disturbances radiating onto a flat plate with a sharp leading edge in the Mach 6 free stream is carried out. Numerical data obtained for fast and slow acoustic waves of zero angle of incidence are consistent with the asymptotic theory. Numerical experiments with acoustic waves of non-zero angles of incidence reveal new features of the disturbance field near the plate leading edge. The shock wave, which is formed near the leading edge owing to viscous–inviscid interaction, produces a profound effect on the acoustic near field and excitation of boundary-layer modes. DNS of the porous coating effect on stability and receptivity of the hypersonic boundary layer is carried out. A porous coating of regular porosity (equally spaced cylindrical blind micro-holes) effectively diminishes the second-mode growth rate in accordance with the predictions of linear stability theory, while weakly affecting acoustic waves. The coating end effects, associated with junctures between solid and porous surfaces, are investigated.

1. Introduction

Prediction of laminar–turbulent transition is important for aerothermal design and drag calculations of high-speed vehicles (Reed *et al.* 1997). This motivates experimental, theoretical and numerical studies of transition at supersonic and hypersonic speeds. Progress made in the transition prediction methodology is reviewed by Malik, Zang & Bushnell (1990) and Malik (1997). There are at least two routes to turbulent flow in the boundary layer. The first route, which occurs in 'quiet' free streams on aerodynamically smooth surfaces, includes receptivity, linear phase and nonlinear breakdown to turbulence (Morkovin 1969). Receptivity refers to the mechanism by which free-stream disturbances enter the laminar boundary layer and generate unstable waves (Reshotko 1976). The linear phase is associated with amplification of unstable disturbances, which are described by the linear stability theory (LST). The nonlinear breakdown occurs when the disturbance amplitudes achieve a certain critical level. The second route of transition is observed in 'noisy' environments and is associated with the bypassing of the linear phase. The receptivity process is poorly understood, especially at supersonic and hypersonic speeds. This prevents us from developing rational transition prediction methods, which couple the transition locus with characteristics of free-stream disturbances and avoid the empiricism of the e^N-method (Malik *et al.* 1990).

Theoretical studies of Mack (1969) and stability experiments of Demetriades (1974), Kendall (1975) and Stetson *et al.* (1991) showed that evolution of disturbances in

supersonic boundary layers on a sharp cone and flat plate is essentially different from the case of subsonic flows. Besides the first mode associated with Tollmien–Schlichting waves, there are the second and higher modes relevant to the family of trapped acoustic waves (Mack 1969; Guschin & Fedorov 1989). The second mode becomes the dominant instability mode at sufficiently high Mach numbers M (for the boundary layer on an insulated wall at zero pressure gradient, this occurs for $M > 4$). In contrast to the first mode, the growth rate of the second mode is maximal for two-dimensional waves. This facilitates the modelling of the receptivity and instability phases associated with the second mode.

Fedorov & Khokhlov (1991, 1993, 2001) developed a theoretical model of receptivity to acoustic disturbances radiating over the sharp leading edge of a flat plate in supersonic flow. This model provides insight into the physics of the receptivity process associated with diffraction and scattering of acoustic waves in the leading-edge vicinity. The boundary-layer mode excited near the leading edge by a fast acoustic wave can be referred as mode F, and by a slow acoustic wave as mode S. The theoretical predictions (Fedorov 2003) of receptivity coefficients agree well with the experimental data of Maslov *et al.* (2001), which were obtained in the Mach 6 wind tunnel. They are also consistent with the direct numerical simulations (DNS) of Ma & Zhong (2001).

Unfortunately, the experiments of Maslov *et al.* (2001) provide, to our knowledge, the only set of data, which could be used for direct verification of theoretical models dealing with receptivity of high-speed flows. Reliable numerical experiments seem to be the only way to acquire detailed data on the disturbance evolution in various phases of transition. This explains the high interest in DNS of disturbances in boundary layers at supersonic and hypersonic speeds. Zhong (2001) and Ma & Zhong (2003*a*, *b*) conducted a series of numerical studies related to receptivity and stability of high-speed flows over a parabolic leading edge and a flat plate. Two-dimensional DNS of receptivity to acoustic waves was carried out by Ma & Zhong (2003*b*) using a high-order shock-fitting scheme. However, this scheme is not applicable to a small region near the leading edge, which may play an important role in receptivity, especially when acoustic waves radiate over the leading edge from below (Fedorov & Khokhlov 1993; Fedorov 2003). Seemingly, this explains why Ma & Zhong considered acoustic waves radiating over the plate from above or at zero angle of incidence and did not treat the radiation from below. Balakumar, Zhao & Atkins (2002) numerically investigated the stability of a hypersonic boundary layer over a compression corner using a high-order weighted essentially non-oscillatory (WENO) shock-capturing scheme.

Though aforementioned papers provide a great deal of data, further DNS studies are needed to confirm previous numerical results and consider the disturbance evolution from new perspectives. In this paper, we discuss DNS of receptivity to slow and fast acoustic waves radiating over a flat plate in a Mach 6 free stream. The two-dimensional unsteady compressible Navier–Stokes equations are solved using the second-order shock-capturing TVD scheme, which allows for sufficiently accurate simulation of scattering and diffraction of acoustic disturbances in the leading-edge vicinity. Stability characteristics predicted by this method agree well with the LST calculations performed for the boundary layer on a flat plate in a Mach 6 free stream (Egorov, Fedorov & Soudakov 2006). The present paper shows that numerical data obtained in the case of fast and slow acoustic waves with zero angle of incidence are consistent with the theoretical results of Fedorov & Khokhlov (1991, 1993, 2001) and the DNS of Ma & Zhong (2003*b*). Numerical experiments conducted for acoustic

waves of the angles of incidence $\pm 45^\circ$ reveal new features of the disturbance field in the leading-edge vicinity, which are important in the receptivity process.

Besides modelling of transition phases, it is of practical importance to control hypersonic laminar flows (Kimmel 2003). Smoothing and shaping of the vehicle surface help to avoid early transition due to roughness, leading-edge contamination as well as cross-flow and Görtler instabilities. However, with these measures the laminar run may still be short because of the first and/or second mode instability. The nose bluntness can be used to control these modes by changing the entropy layer and the local Mach number. However, bluntness leads to a significant increase of the wave drag. The first mode can be stabilized by the wall cooling, suction and favourable pressure gradient (Gaponov & Maslov 1980). In contrast to the first mode, the wall cooling destabilizes the second mode (Malik 1989). Because the surface temperature of typical high-speed vehicles is essentially lower than the adiabatic wall temperature, instability of the first mode is suppressed naturally, whereas the second mode grows faster and can lead to relatively earlier transition. This indicates that hypersonic laminar flow control concepts should address the second-mode instability.

Because the second mode represents high-frequency (ultrasonic) trapped acoustic waves, Malmuth *et al.* (1998) assumed that a passive ultrasonically absorptive coating (UAC) may stabilize this mode and, at the same time, may be aerodynamically smooth. This hypothesis was confirmed by linear stability calculations in inviscid (Malmuth *et al.* 1998) and viscous (Fedorov *et al.* 2001) approximations. It was shown that a relatively thin porous layer causes massive decreasing of the second-mode growth rate. Experiments of Rasheed *et al.* (2002), which were performed on a sharp cone at zero angle of attack in high-enthalpy flow of Mach number 4.6–6.4, qualitatively confirmed the theoretical predictions. For the majority of runs, the boundary layer on the porous surface (comprising equally spaced cylindrical blind micro-holes) was laminar up to the model base, while transition on the untreated solid surface was observed at halfway along the cone. These results motivated stability experiments on cones with different porous coatings.

The first series of stability measurements (Fedorov *et al.* 2003*b*) was carried out in the Mach 6 wind tunnel. The tested model was a sharp cone with a UAC of fibrous absorbent material (felt metal). Hot-wire measurements and LST calculations showed that this coating effectively stabilizes the second mode while it destabilizes low-frequency disturbances relevant to the first mode. The second series of experiments (Fedorov *et al.* 2003*a*) was conducted on a similar cone model with a UAC of regular microstructure (a perforated thin sheet which is analogous to that used in the experiments of Rasheed *et al.* 2002). This coating also stabilized the second mode and weakly affected the first mode. Measured phase speeds and amplitudes of boundary-layer disturbances agree satisfactorily with the LST calculations. Nonlinear aspects of the second mode stabilization by a UAC of regular microstructure were treated by Bountin *et al.* (2004) using bispectral analysis. It was shown that the harmonic resonance, which is pronounced in the latter stages of the disturbance evolution on solid surfaces, is completely suppressed on the porous surface. Malsov *et al.* (2006) carried out experiments in the Mach 12 high-enthalpy wind tunnel, showing that the felt-metal coating significantly (up to 100% of the model length) delayed transition.

Aforementioned studies confirmed the UAC laminar flow control concept. However, more accurate modelling of the UAC performance is still required. In previous works, stability calculations were carried out using LST for local-parallel or weakly non-parallel flows. The mean flow was approximated by the self-similar (compressible Blasius) solutions for a flat plate or sharp cone; i.e. the viscous–inviscid interaction

was neglected. Non-uniformity of boundary conditions due to the UAC end effects (upstream and downstream boundaries of the coating) was not considered. Sudden changes of the surface boundary conditions may act as additional receptivity sites that may reduce the UAC performance. Interaction of external disturbances (acoustic, vorticity and entropy waves) with the porous surface was not analysed. These aspects are addressed herein using direct numerical simulation of disturbance fields over a flat plate in a hypersonic free stream of Mach number 6. Calculations are carried out for two-dimensional disturbances generated by fast and slow acoustic waves of various angles of incidence. The boundary conditions on the porous surface are formulated using the theoretical model of Fedorov *et al.* (2001).

2. Problem formulation

Viscous unsteady compressible flows are governed by Navier–Stokes equations. For two-dimensional flows, these equations are written in the conservative non-dimensional form

$$\frac{\partial \boldsymbol{Q}}{\partial t} + \frac{\partial \boldsymbol{E}}{\partial \xi} + \frac{\partial \boldsymbol{G}}{\partial \eta} = 0,$$

where (ξ, η) is a curvilinear coordinate system, $x = x(\xi, \eta)$, $y = y(\xi, \eta)$ are Cartesian coordinates, $\boldsymbol{Q}$ is a vector of dependent variables, $\boldsymbol{E}$ and $\boldsymbol{G}$ are flux vectors in the (ξ, η) coordinate system. These vectors are expressed in terms of the corresponding vectors $\boldsymbol{Q}_c$, $\boldsymbol{E}_c$, $\boldsymbol{G}_c$ in the Cartesian coordinate system as

$$\boldsymbol{Q} = J\,\boldsymbol{Q}_c, \quad \boldsymbol{E} = J\left(\boldsymbol{E}_c\frac{\partial \xi}{\partial x} + \boldsymbol{G}_c\frac{\partial \xi}{\partial y}\right), \quad \boldsymbol{G} = J\left(\boldsymbol{E}_c\frac{\partial \eta}{\partial x} + \boldsymbol{G}_c\frac{\partial \eta}{\partial y}\right),$$

where $J = \det\|\partial(x, y)/\partial(\xi, \eta)\|$ is the transformation Jacobian. Cartesian vector components for two-dimensional Navier–Stokes equations are

$$\boldsymbol{Q}_c = \begin{bmatrix} \rho \\ \rho u \\ \rho v \\ e \end{bmatrix}, \quad \boldsymbol{E}_c = \begin{bmatrix} \rho u \\ \rho u^2 + p - \dfrac{1}{Re_\infty}\tau_{xx} \\ \rho u v - \dfrac{1}{Re_\infty}\tau_{xy} \\ \rho u H - \dfrac{1}{Re_\infty}\left(u\tau_{xx} + v\tau_{xy} + \dfrac{\mu}{Pr\,(\gamma-1)\,M_\infty^2}\dfrac{\partial T}{\partial x}\right) \end{bmatrix}$$

$$\boldsymbol{G}_c = \begin{bmatrix} \rho v \\ \rho u v - \dfrac{1}{Re_\infty}\tau_{xy} \\ \rho v^2 + p - \dfrac{1}{Re_\infty}\tau_{yy} \\ \rho v H - \dfrac{1}{Re_\infty}\left(u\tau_{xy} + v\tau_{yy} + \dfrac{\mu}{Pr\,(\gamma-1)\,M_\infty^2}\dfrac{\partial T}{\partial y}\right) \end{bmatrix}$$

Here, ρ is density; u, v are Cartesian components of the velocity vector $\boldsymbol{V}$; p is pressure; T is temperature; $e = p/(\gamma-1) + \rho(u^2+v^2)/2$ is total energy; $H = T/((\gamma-1)M_\infty^2) + (u^2+v^2)/2$ is total specific enthalpy; τ is stress tensor with components

$$\tau_{xx} = \mu\left(-\tfrac{2}{3}\mathrm{div}\boldsymbol{V} + 2\frac{\partial u}{\partial x}\right), \quad \tau_{xy} = \mu\left(\frac{\partial u}{\partial y} + \frac{\partial v}{\partial x}\right), \quad \tau_{yy} = \mu\left(-\tfrac{2}{3}\mathrm{div}\boldsymbol{V} + 2\frac{\partial v}{\partial y}\right).$$

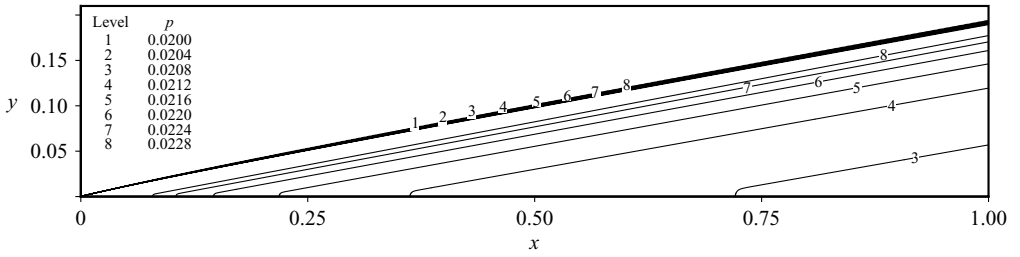

FIGURE 1. Pressure contours in the computational domain.

The fluid is a perfect gas with the specific heat ratio $\gamma = 1.4$ and Prandtl number $Pr = 0.72$. The system of equations is closed by state equation $p = \rho T/(\gamma M_\infty^2)$. The viscosity–temperature dependence is approximated by the power law $\mu^*/\mu_\infty^* = (T^*/T_\infty^*)^{0.7}$. The second viscosity is assumed to be zero.

Numerical studies are carried out for hypersonic flow over a flat plate at the free-stream Mach number $M_\infty = 6$ and the Reynolds number $Re_\infty = \rho_\infty^* U_\infty^* L^*/\mu_\infty^* = 2 \times 10^6$, where ρ_∞^* is free-stream density, U_∞^* is free-stream velocity and L^* is plate length. Hereinafter, asterisks denote dimensional variables. Flow variables are made non-dimensional using the steady-state free-stream parameters as $(u, v) = (u^*, v^*)/U_\infty^*$, $p = p^*/(\rho_\infty^* U_\infty^{*2})$, $\rho = \rho/\rho_\infty^*$, $T = T^*/T_\infty^*$. The non-dimensional coordinates and time are $(x, y) = (x^*, y^*)/L^*$, $t = t^* U_\infty^*/L^*$.

The plate has a nominally sharp leading edge; i.e. the leading-edge radius r^* is so small that the bluntness-induced entropy layer does not affect receptivity and stability of the boundary layer. In accordance with the asymptotic theory (Fedorov 2003; Egorov, Fedorov & Nechaev 2004), this is valid for the bluntness Reynolds number $Re_b = \rho_\infty^* r^* U_\infty^*/\mu_\infty^* \ll F^{-3/4}$, where $F = \omega^* \mu_\infty^*/\rho_\infty^* U_\infty^{*2}$ is the frequency parameter. Typically, F is less than 10^{-4} which gives the restriction $Re_b = \rho_\infty^* r^* U_\infty^*/\mu_\infty^* \ll 10^3$.

The boundary conditions on the solid wall ($y = 0$) are: no-slip condition $(u, v) = 0$; $\partial T_w/\partial y = 0$ corresponding to the adiabatic wall temperature. The boundary conditions on the porous surface are discussed in § 4. On the outflow boundary, the unknown variables u, v, p, T are extrapolated using a linear approximation. On inflow and upper boundaries, conditions correspond to an undisturbed free stream. Details on the problem formulation and governing equations are given by Egorov *et al.* 2006.

The problem is solved numerically using the implicit second-order finite-volume method described by Egorov *et al.* (2006). Two-dimensional Navier-Stokes equations are approximated by a TVD shock-capturing scheme. This is of particular importance for simulation of receptivity processes in which free-stream disturbances pass through the shock and induce its oscillations. The shock-capturing scheme allows for modelling of the disturbance dynamics in the leading-edge vicinity, where receptivity to free-stream disturbances is most pronounced. Nevertheless, this computational scheme damps physical waves, especially near the peaks and valleys. The numerical dissipation can be suppressed using sufficiently fine computational grids. Egorov *et al.* (2006) carried out DNS of disturbances generated by a local periodic suction-blowing in the boundary layer on a flat plate at the free-stream parameters considered herein. They showed that the grid of 1501×201 nodes (with clustering in the boundary layer and leading-edge region) is appropriate for modelling of the boundary-layer instability. Namely, the calculated second-mode growth rate agreed well with that predicted by LST. With this reasoning, the aforementioned computational grid is used for the DNS discussed hereinafter.

At first, the steady-state solution, which satisfies the undisturbed free-stream boundary conditions on inflow and upper boundaries, is calculated to provide the

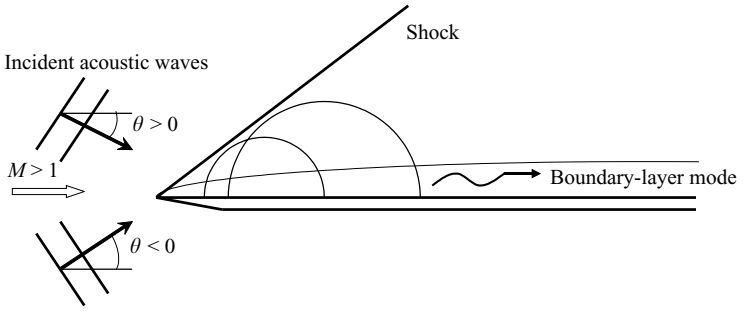

FIGURE 2. Sketch of receptivity of free-stream acoustic waves interacting with a supersonic flow over a flat plate.

mean laminar flow. The steady pressure field shown in figure 1 indicates that the viscous–inviscid interaction of the boundary layer with the free stream leads to the formation of a shock wave emanating from the plate leading edge. As will be shown below, this shock plays an important role in the receptivity process, especially near the leading edge.

3. Receptivity to acoustic disturbances

For modelling of receptivity to acoustic disturbances, a plain monochromatic acoustic wave is imposed on the free stream (figure 2) as

$$(u', v', p', T')_\infty^T = (|u'|, |v'|, |p'|, |T'|)_\infty^T \exp[\mathrm{i}(k_x x + k_y y - \omega t)], \tag{1}$$

where $|u'|$, $|v'|$, $|p'|$, $|T'|$ are dimensionless amplitudes

$$\left.\begin{aligned} &|p'| = \varepsilon, \quad |u'| = \pm M_\infty |p'| \cos\theta, \\ &|v'| = \mp M_\infty |p'| \sin\theta, \quad |T'| = (\gamma - 1) M_\infty^2 |p'|, \end{aligned}\right\}. \tag{2}$$

the upper (lower) sign corresponds to the fast (slow) acoustic wave. The angle of incidence θ is positive (negative) if the acoustic wave radiates over the plate from above (below); ε is the amplitude of the incident wave; $k_x = k_\infty \cos\theta$, $k_y = -k_\infty \sin\theta$ are wavenumber components; $\omega = \omega^* L^*/U_\infty^*$ – circular frequency. The wavenumber is expressed as $k_\infty = \omega M_\infty/(M_\infty \cos\theta \pm 1)$. If the angle of incidence is zero, $\theta = 0°$, then

$$k_x = k_\infty, \; k_y = 0, \quad |u'| = \pm M_\infty |p'|, \; |v'| = 0, \; |p'| = \varepsilon, \; |T'| = (\gamma - 1) M_\infty^2 |p'|.$$

For positive θ (radiating from above), these relations are imposed on the inflow and upper boundary. For negative θ (radiating from below), the acoustic wave is specified on the inflow boundary whereas special boundary conditions (buffer zone with grid stretching and 'soft' conditions) are imposed on the upper boundary.

Herein we consider acoustic waves of small amplitude $\varepsilon = 5 \times 10^{-5}$ at which the receptivity process is linear. The disturbance frequency $\omega = 260$ corresponds to the frequency parameter $F = \omega/Re = 1.3 \times 10^{-4}$. At this frequency, the maximum amplitude predicted by LST is observed at the station $x \approx 0.9$ and associated with the second-mode wave. The temperature disturbance is zero on the plate surface, $T'|_{y=0} = 0$. Calculations are performed for the angles of incidence $\theta = 0°, \pm 45°$.

3.1. *Acoustic disturbances of zero angle of incidence*

In the case of $\theta = 0°$, the pressure disturbance field (difference between an instantaneous flow field and the mean flow field) induced by the fast (slow) wave is

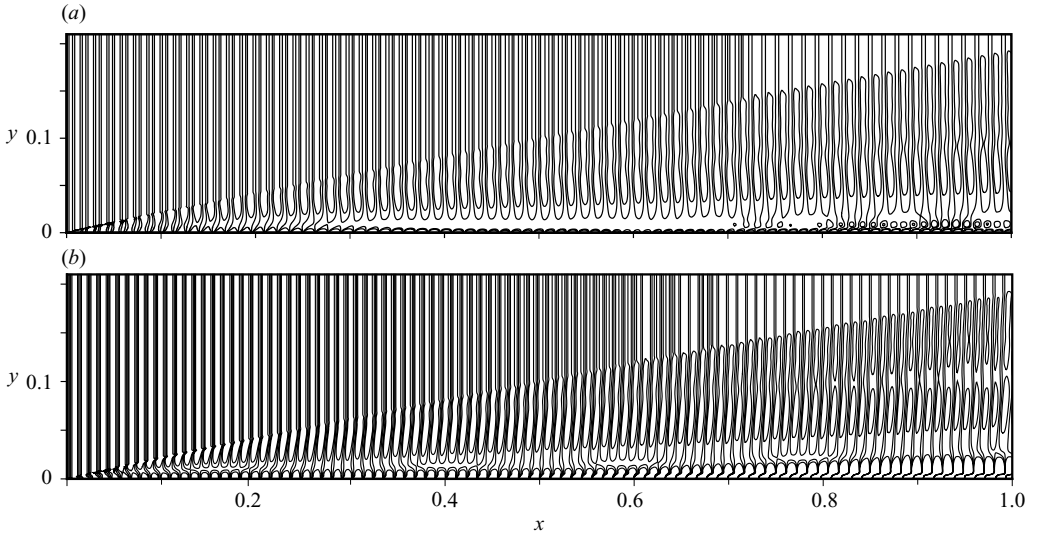

FIGURE 3. The pressure disturbance field induced by (*a*) fast and (*b*) slow acoustic wave of zero angle of incidence.

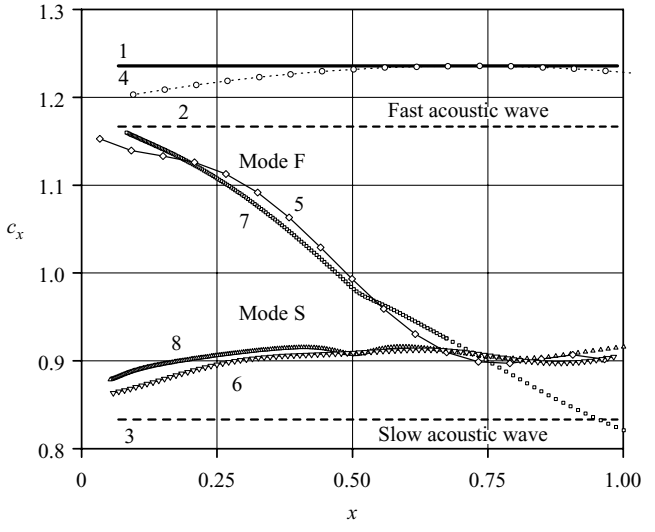

FIGURE 4. Disturbance phase speeds: 1, fast acoustic wave of $\theta = +45^\circ$; 2, fast acoustic wave of $\theta = 0^\circ$; 3, slow acoustic wave of $\theta = 0^\circ$; 4, disturbances induced in the boundary layer by a fast acoustic wave of $\theta = +45^\circ$ (DNS); 5, disturbances induced in the boundary layer by a fast acoustic wave of $\theta = 0^\circ$ (DNS); 6, disturbances induced in the boundary layer by a slow acoustic wave of $\theta = 0^\circ$ (DNS); 7, disturbances induced in the boundary layer by a fast acoustic wave of $\theta = 0^\circ$ (LST); 8, disturbances induced in the boundary layer by slow acoustic wave of $\theta = 0^\circ$ (LST).

shown in figure 3*a* (3*b*). The shock wave weakly disturbs the acoustic field pattern. Nevertheless, the acoustic wave amplitude behind the shock is changed, as will be shown in § 3.2. Major distortions are observed in the near-wall region and associated with the interaction of acoustic disturbances with the boundary layer.

It is convenient to interpret the disturbance evolution using the phase speed distributions $c_x(x)$ of different modes (figure 4). The dashed lines 2 and 3 show

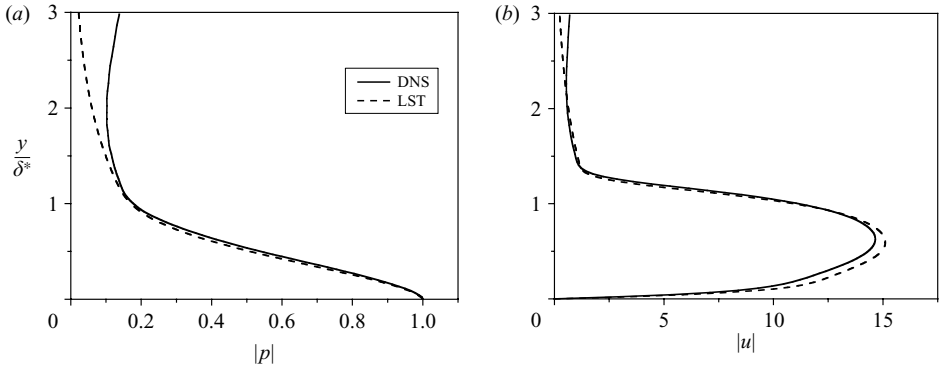

FIGURE 5. Distributions of (*a*) pressure and (*b*) *u*-velocity disturbances across the boundary layer at the station $x = 0.3$; solid line, disturbance induced by fast acoustic wave of $\theta = 0°$ (DNS); dashed line, eigenfunction of the mode F (LST); the disturbance is normalized by the wall pressure.

the lower bound ($c_x = 1 + 1/M_\infty$) for fast acoustic waves and the upper bound ($c_x = 1 - 1/M_\infty$) for slow acoustic waves, respectively. These bounds correspond to zero angle of incidence, $\theta = 0°$. Curves 7 and 8 show phase speeds of modes F and S predicted by LST. This terminology was proposed by Fedorov (2003) in connection with the asymptotic behaviour of the mode phase speed in the leading-edge vicinity ($x \to 0$). Namely, the phase speed of mode F (fast mode) tends to the phase speed $c_x = 1 + 1/M_\infty$ of a fast acoustic wave whereas the phase speed of mode S (slow mode) tends to $c_x = 1 - 1/M_\infty$ of a slow acoustic wave. In contrast to the terminology of Mack (1969), the new terminology allows for unambiguous definition of the boundary-layer modes at hypersonic speeds. This issue is also discussed by Forgoston & Tumin (2005). In the case considered herein, the mode S corresponds to the Mack first mode upstream from the synchronization point ($x \approx 0.7$), and to the Mack second mode downstream from this point. Note that LST results shown in figure 4 were obtained using the self-similar mean-flow solution, which was calculated with the upper boundary-layer edge parameters taken from the DNS steady-state solution. The phase speed distributions predicted by DNS are approximately calculated using the wall pressure disturbance $p_w(x)$: $c_x(x) \approx \omega \Delta x / \pi$, where Δx is the distance between neighbouring zeros of the function $p_w(x)$. Mean lines of these distributions are shown in figure 4.

3.1.1. *Fast acoustic wave*

Consider a fast acoustic wave radiating over the plate at $\theta = 0°$. The phase speed of mode F predicted by LST (curve 7 in figure 4) is close to the DNS solution (curve 5) in the range $0 < x < 0.5$. This indicates that the mode F is dominant in the boundary layer. Comparison of the mode F eigenfunction predicted by LST with the DNS distributions (figure 5) confirms this statement. Within the boundary layer $0 < y < 1.5\delta^*$ (δ^* is the boundary-layer displacement thickness), the DNS solution agrees with the mode F eigenfunction. In the outer flow, the discrepancy is due to the presence of an acoustic wave in the disturbance field predicted by DNS. One-cell structures in the pressure disturbance field near the wall (figure 6*a*) also indicate that the mode F is dominant in the considered range of x. Effective excitation of the mode F is due to synchronization of this mode with the fast acoustic wave near the leading edge (in figure 4, curve 5 tends to line 2 as $x \to 0$). This synchronization leads to a

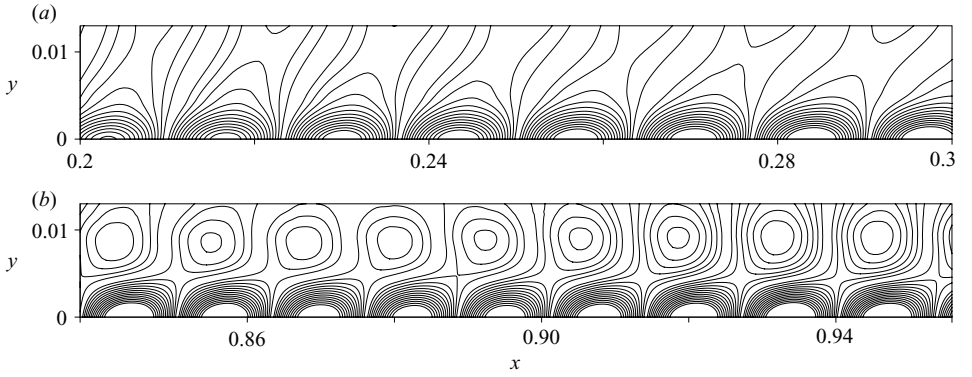

FIGURE 6. Details of the pressure disturbance field induced by fast acoustic wave of zero angle of incidence, (*a*) $0.2 < x < 0.3$; (*b*) $0.85 < x < 0.95$.

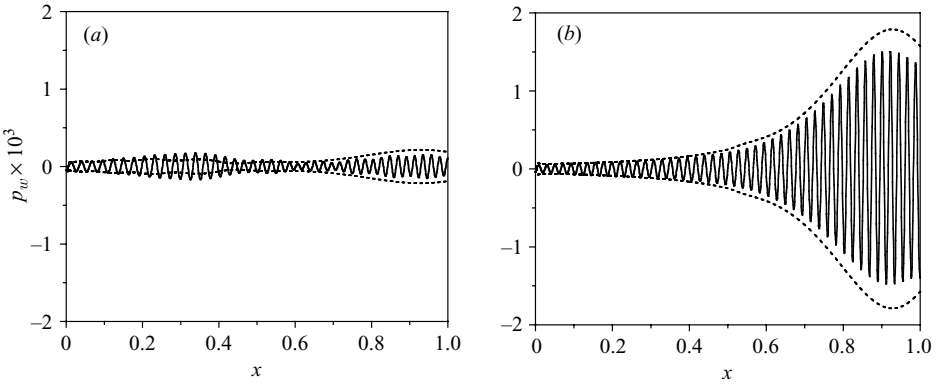

FIGURE 7. Wall pressure disturbances induced by (*a*) fast and (*b*) slow acoustic wave of $\theta = 0°$: solid line, DNS; dashed line, theory.

monotonic increase of the mode F amplitude in the region $0 < x < 0.35$ (see the wall pressure disturbances in figure 7*a*).

Further downstream, the phase speed of mode F decreases (figure 4, curve 5) detuning the synchronization conditions, the excitation weakens and the mode F slowly attenuates (figure 7*a*, $0.35 < x < 0.5$). Then, mode F is synchronized with mode S and excites the latter via the inter-modal exchange mechanism described by Fedorov & Khokhlov (2001). This occurs somewhere in the range $0.5 < x < 0.7$. The presence of two modes with different wavenumbers leads to beats of the disturbance amplitude (figure 7*a*). Further downstream, $0.7 < x < 1$, the mode S amplifies due to its instability (figure 7*a*) and forms a two-cell structure in the pressure disturbance field observed in the boundary layer (figure 6*b*).

Another insight into the disturbance evolution is given by instantaneous contours of the density disturbance shown in figures 8 and 9. In the boundary layer, these contours form a street of cells. For $x < 0.7$, neighbouring cells are separated from each other which is typical for mode F (a detailed fragment of this structure is shown in figure 9*a* for $0.2 \leqslant x \leqslant 0.3$). As the disturbance evolves downstream, cells crowd and ultimately overlap forming a rope-like structure in the range $0.8 < x < 1$ (typical for mode S). Figure 9(*b*) shows that this structure is located in the critical layer, where the mean-flow velocity is close to the disturbance phase speed. Note that the density

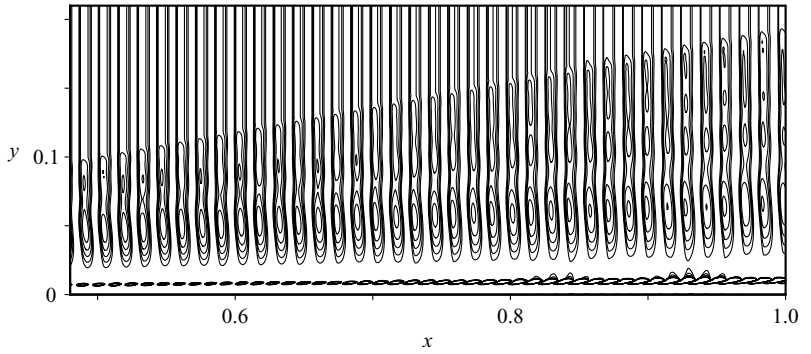

FIGURE 8. The density disturbance field induced by fast acoustic wave of zero angle of incidence.

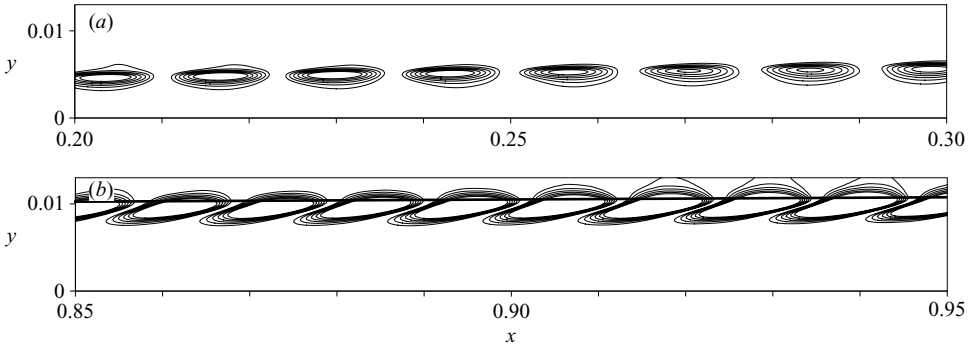

FIGURE 9. The density disturbance field induced by fast acoustic wave of zero angle of incidence: (*a*) Mode F; (*b*) Mode S. The thick solid line shows the locus of the critical point at which the mean-flow velocity is equal to the disturbance phase speed.

contour pattern in figure 8 is similar to that calculated by Ma & Zhong (2003*b*, figure 2).

The aforementioned scenario is consistent with that predicted theoretically by Fedorov & Khokhlov (1991, 1993). This motivates us to perform calculations of the wall pressure disturbance using the theoretical model of leading-edge receptivity (Fedorov & Khokhlov 1993) and the two-mode approximation (Fedorov 2003). Namely, the boundary-layer disturbance is expressed as a sum of two eigensolutions with unknown amplitude coefficients $C_{1,2}(x)$. These eigensolutions correspond to the modes F and S. The coefficients $C_{1,2}(x)$ are governed by the system of two ordinary differential equations, which accounts for the interaction between modes owing to non-parallel effects. The initial values of amplitude coefficients (for $x \to 0$) are determined using the analytical solution (Fedorov & Khokhlov 1993) of the leading-edge receptivity problem. Then, the Cauchy problem for $C_{1,2}(x)$ is solved numerically. Details of this approach are given by Fedorov (2003). Note that in this theoretical model the distributed excitation of boundary-layer modes by the incident acoustic wave (that may occur downstream from the leading-edge region) is neglected. In addition, the theory does not account for the interaction of incident acoustic waves with the shock. The theoretical distribution of the wall pressure amplitude is shown by the dashed line in figure 7(*a*). Despite of the aforementioned deficiencies, the theory captures basic features of the DNS solution.

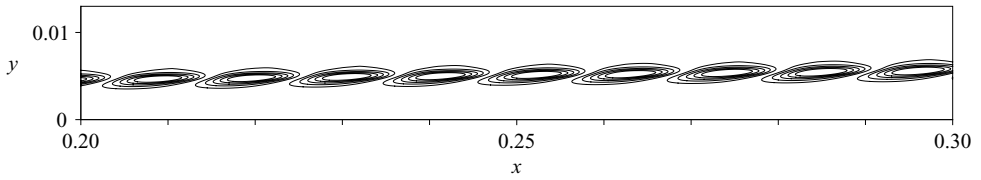

FIGURE 10. Density disturbance field near the leading edge induced by slow acoustic wave of zero angle of incidence.

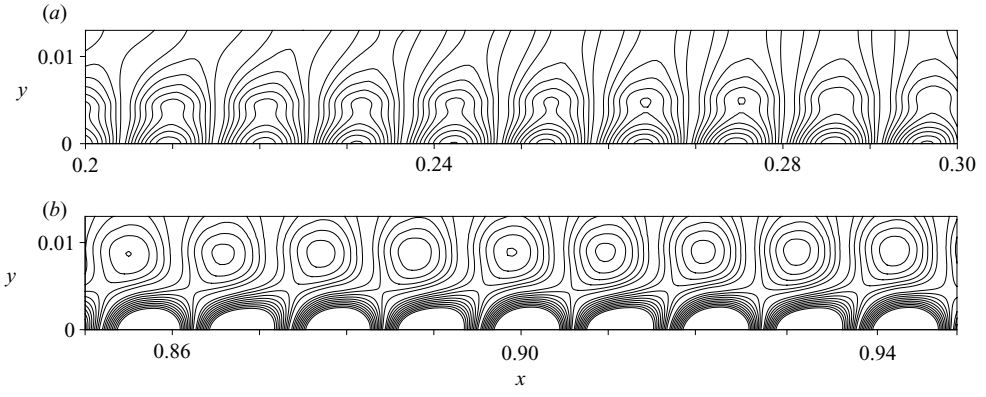

FIGURE 11. Details of the pressure disturbance field induced by slow acoustic wave of zero angle of incidence: (*a*) $0.2 < x < 0.3$; (*b*) $0.85 < x < 0.95$.

3.1.2. *Slow acoustic wave*

The theoretical model of Fedorov & Khokhlov (1991, 1993) indicates that receptivity to the slow acoustic wave of $\theta = 0^\circ$ is essentially different from the case of the fast acoustic wave. The slow wave is directly synchronized with mode S near the leading edge (see curves 3 and 6 in figure 4). This leads to an algebraic ($\sim x^{1/4}$) growth of the mode S amplitude. The theoretical findings are consistent with DNS. Detailed examination of the disturbance field in the boundary layer does not show any evidence of mode F, whereas mode S is clearly recognized starting from the leading-edge region. As an example, figure 10 shows the density disturbance in the range $0.2 \leqslant x \leqslant 0.3$. Neighbouring maximums and minimums overlap, forming a rope-like structure indicating that mode S is dominant in this region. The corresponding pressure field is shown in figure 11(*a*). Furthermore, the DNS distributions of pressure and u-velocity disturbances across the boundary layer are close to the mode S eigenfunction predicted by LST (figure 12, $x = 0.3$).

Downstream from $x \approx 0.6$, mode S is related to the Mack second mode and amplifies intensively. This is accompanied by the formation of two-cell structures in the disturbance pressure field (figure 11*b*). As shown in figure 13, the DNS solution agrees with the LST eigenfunction in the station $x = 0.9$.

These numerical results are consistent with the theoretical model described in § 3.1.1. The theoretical distribution of the wall pressure amplitude (dashed line in figure 7*b*) agrees with the DNS solution.

Other interesting features of the disturbance field are observed for both fast and slow acoustic waves outside the boundary layer. Figure 3 shows that, for $x > 0.2$, the pressure amplitude is relatively small in a layer that occurs just above the boundary

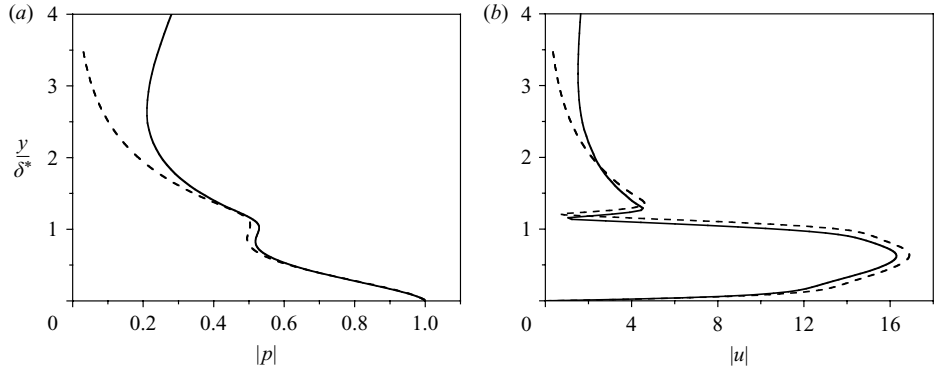

FIGURE 12. Distributions of (*a*) pressure and (*b*) *u*-velocity disturbances across the boundary layer at the station $x = 0.3$: solid line, disturbance induced by slow acoustic wave of $\theta = 0°$ (DNS); dashed line, eigenfucntion of the mode S (LST); the disturbance is normalized by the wall pressure.

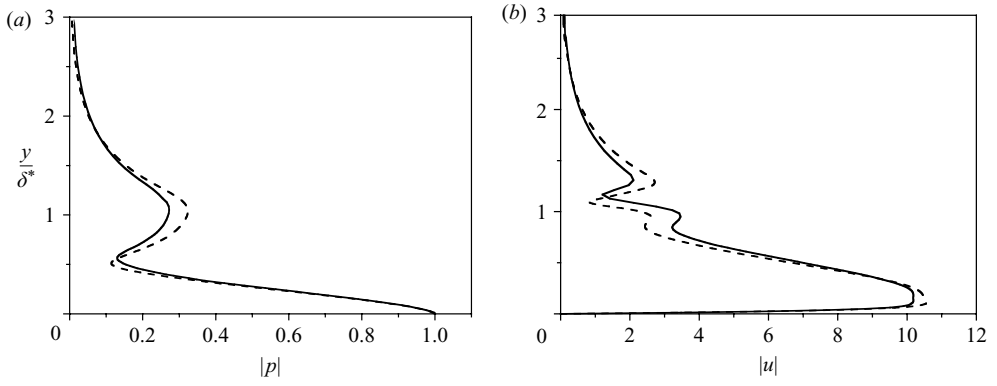

FIGURE 13. Distributions of (*a*) pressure and (*b*) *u*-velocity disturbances across the boundary layer at the station $x = 0.9$; solid line, disturbance induced by slow acoustic wave of $\theta = 0°$ (DNS); dashed line, eigenfucntion of the mode S (LST); the disturbance is normalized by the wall pressure.

layer and grows downstream. This 'quiet' layer separates the external acoustic field from boundary-layer disturbances in a way that is consistent with the theoretical prediction of Fedorov & Khokhlov (1991, 1993) for acoustic disturbances in the diffraction zone. Very close to the leading edge ($x < 0.2$) there is a shock layer, which may be treated as an acoustic waveguide. The pressure field in this region resembles the analytical solution of Guschin & Fedorov (1989) describing wave-guide modes in a thin shock layer.

3.2. *Acoustic disturbances of non-zero angles of incidence*

Numerical experiments with fast and slow acoustic waves of $\theta = +45°$ (radiating from above) and $\theta = -45°$ (radiating from bellow) reveal new features of leading-edge receptivity, which were not captured by the asymptotic theory of Fedorov & Khokhlov (1991, 1993, 2001). They are associated with the interaction of incident acoustic waves with the shock wave induced by the plate. Acoustic waves passing through the shock change their amplitude and generate entropy and vorticity waves behind the shock

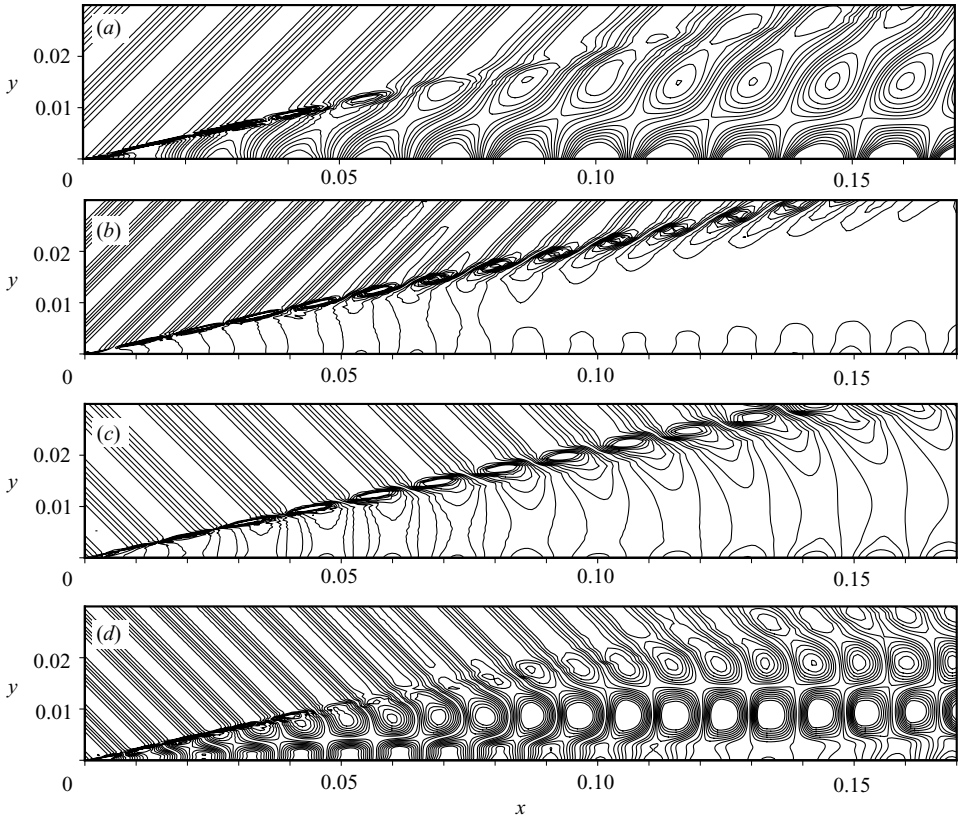

FIGURE 14. The pressure disturbance field induced by (*a*) fast and (*b*) slow acoustic waves of $\theta = +45^\circ$ and by (*c*) fast and (*d*) slow acoustic wave of $\theta = -45^\circ$; contours are shown from -8×15^{-5} to 8×10^{-5} with step 1×10^{-5}.

(Djakov 1957; McKenzie & Westphal 1968). These effects may change the disturbance field in the shock layer, especially near the leading edge where the viscous–inviscid interaction is appreciable.

Figure 14 shows pressure disturbance fields induced by fast and slow acoustic waves of $\theta = \pm 45^\circ$ in the leading-edge vicinity. Corresponding distributions of the wall pressure disturbance are shown in figure 15. It is seen that the shock wave and the plate surface are boundaries of a wedge-like waveguide. The incident acoustic wave interacting with the plate and the shock wave generates forced disturbances and waveguide modes of an acoustic nature. The forced disturbances have two components: one is induced by distributed forcing associated with penetration of the acoustic wave through the shock; another is due to scattering of the incident acoustic wave by the plate leading edge. These components are related to the receptivity mechanisms A and B discussed by Fedorov (2003).

The fast acoustic wave radiating over the plate from below ($\theta = -45^\circ$) and the slow acoustic wave radiating over the plate from above ($\theta = +45^\circ$) penetrate weakly through the shock (see figures 14*c* and 14*b* respectively) and the waveguide is relatively quiet. On the contrary, the fast wave radiating over the plate from above ($\theta = +45^\circ$) and the slow wave radiating over the plate from below ($\theta = -45^\circ$) effectively excite the waveguide modes (see cell structures in figure 14*a*, *d*).

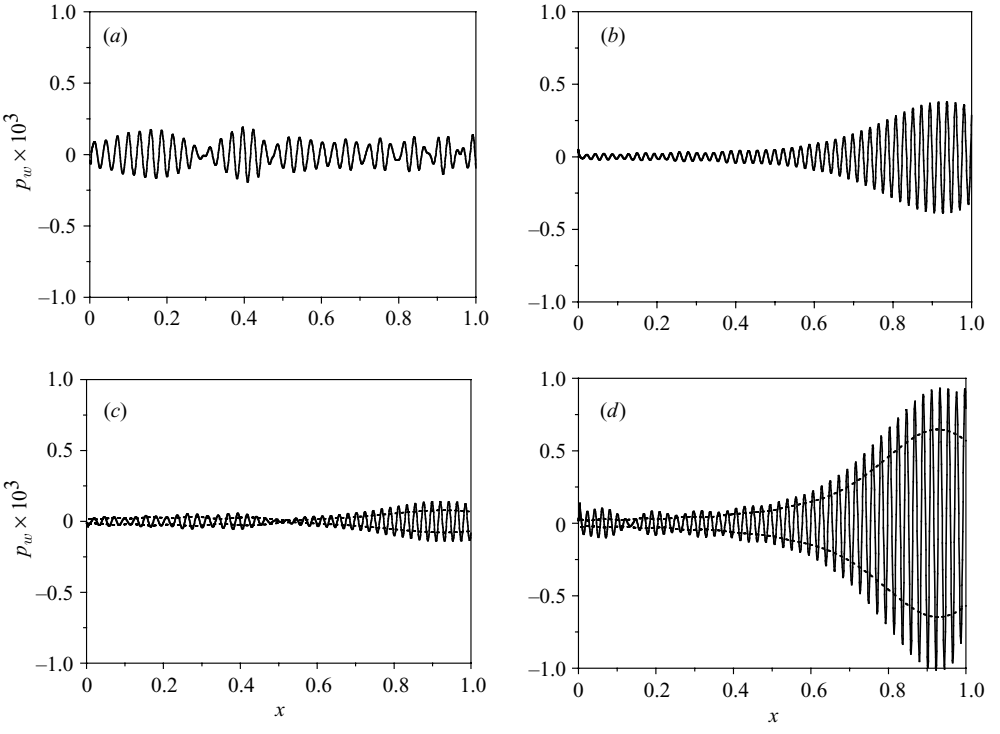

FIGURE 15. Wall pressure disturbances induced by (*a*) fast and (*b*) slow acoustic wave of $\theta = +45°$, (*c*) fast and (*d*) slow acoustic wave of $\theta = -45°$; solid line, DNS; dashed line, theory.

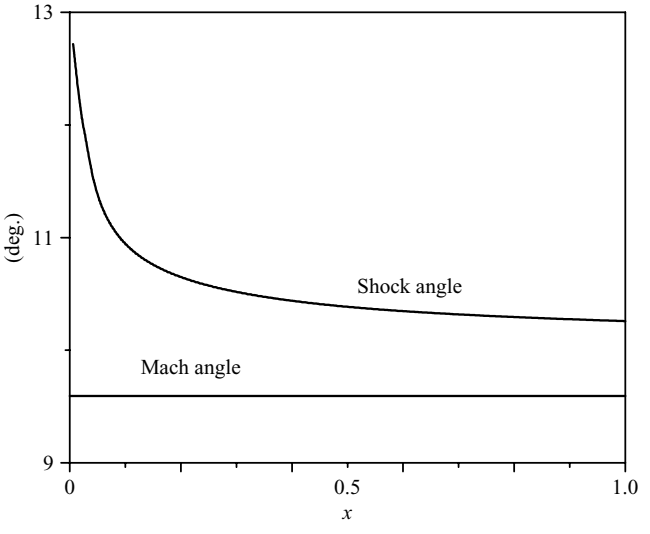

FIGURE 16. Angle of the mean flow shock wave.

These numerical results were analysed using the theoretical model (Djakov 1957; McKenzie & Westphal 1968), which describes penetration of acoustic disturbances through an oblique shock. Figure 16 shows the shock-wave angle corresponding to

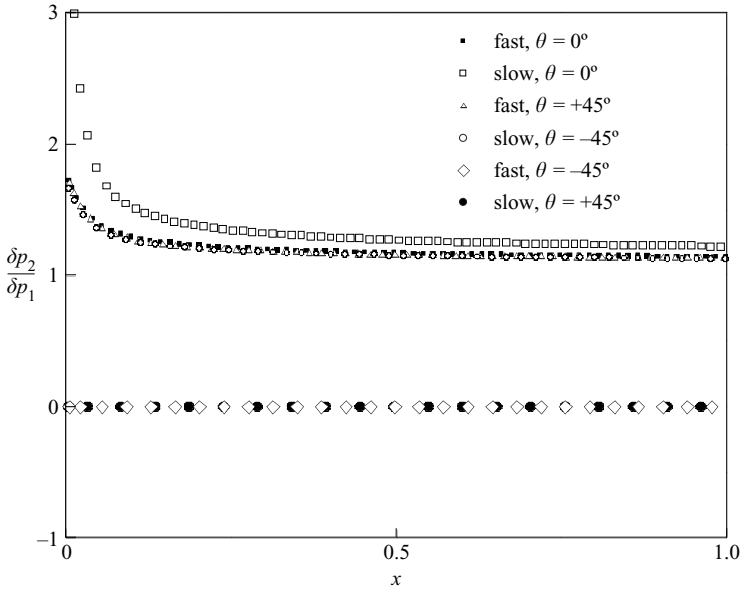

FIGURE 17. Penetration coefficients for various acoustic waves.

the steady-state DNS solution. This angle decreases with the streamwise coordinate to 10.3° at $x = 1$ and slowly approaches the Mach-wave angle 9.6°. These data were incorporated into the analytical solution (Djakov 1957; McKenzie & Westphal 1968) in order to evaluate the local penetration coefficient, which is the ratio of the pressure disturbance amplitude δp_2 just behind the shock to the pressure disturbance amplitude δp_1 of incident wave. Note that the theoretical solution does not account for reflections of acoustic disturbances from the wall and non-uniformities of the mean flow.

Figure 17 shows the penetration coefficient as a function of the streamwise coordinate for slow and fast waves of various angles θ. For the fast wave of $\theta = -45°$ and the slow wave of $\theta = +45°$, the penetration coefficients are zero. This is consistent with DNS predictions (figure 14*c*, *b*) showing weak acoustic field behind the shock. For the fast wave of $\theta = +45°$ and the slow wave of $\theta = -45°$, the penetration coefficients are larger than one. This also correlates with the DNS data (figure 14*a*, *d*) indicating that the acoustic field in the shock layer is stronger than that in the free stream. The penetration coefficients increase towards the plate leading edge; i.e. the leading-edge region is more receptive to the considered acoustic waves. Note that this region was not resolved in the DNS of Ma & Zhong (2003*b*).

Pressure disturbances along the line $y = 0.0287$ are shown in figure 18 (thin line) for the case of a fast acoustic wave with $\theta = +45°$. The bold lines show the analytical solution (Djakov 1957; McKenzie & Westphal 1968). The amplitude jump across the shock agrees with that predicted by the linear theory of Djakov (1957) and McKenzie & Westphal (1968). This comparison indicates that the numerical method is appropriate for the modelling of the interaction between small disturbances and shock waves.

Comparing the wall-pressure amplitudes shown in figure 15*a* (fast wave of $\theta = +45°$) and in figure 15*d* (slow wave of $\theta = -45°$), we conclude that the mode S amplitude in the latter case is essentially larger than that in the former case. Nevertheless, acoustic

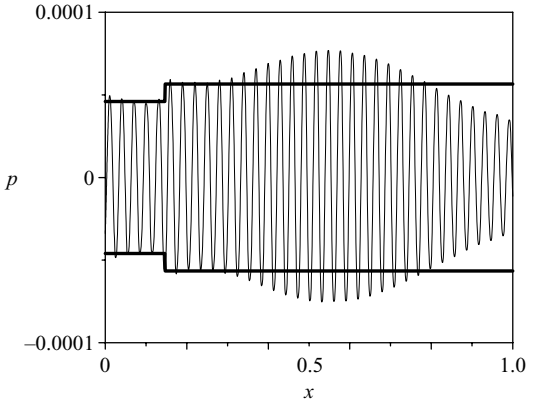

FIGURE 18. The pressure disturbance distribution along the line $y = 0.0287$: thin line, DNS; bold line, linear theory of Djakov (1957) and McKenzie & Westphal (1968).

fields in the shock layer are of approximately the same level (see figure 14a, d). This indicates that excitation of mode S, which is a dominant boundary-layer disturbance in the downstream region, does not depend only on the near-field acoustic level. Another important factor is the difference between the phase speeds of the acoustic wave and mode S. For the slow wave, this difference is relatively small and the coupling between the acoustic field and mode S is stronger than in the case of the fast wave. The same argument explains why receptivity to fast waves is significantly smaller than that to slow waves in all cases presented in figures 7 and 15.

Finally, we discuss the angular dependence of receptivity to slow acoustic waves. At zero angle of incidence, the acoustic near field is synchronized with the mode S and the latter reaches relatively large amplitude in the downstream region. At the positive angle $\theta = +45^\circ$, the acoustic wave weakly penetrates through the shock and the phase difference between mode S and the acoustic disturbance is relatively large. Both effects reduce the receptivity level. At the negative angle $\theta = -45^\circ$, the acoustic wave generates a strong near field with intense acoustic modes in the waveguide, while the phase difference is the same as in the case of $\theta = +45^\circ$. Therefore, maximum pressure disturbance amplitude for the case of $\theta = +45^\circ$ is smaller than that for the case of $\theta = -45^\circ$ (compare figures 15b and 15d).

In the case of receptivity to the fast acoustic wave of $\theta = +45^\circ$, the phase speed of disturbance in the boundary layer (curve 4 in figure 4) is close to that of the acoustic wave $c_x = 1 + 1/(M_\infty \cos 45^\circ)$ (curve 1 in figure 4). There is no evidence of modes F and S. Presumably, their amplitudes are small and the acoustic disturbance dominates in the near-wall region.

Dashed lines in figure 15(c, d) show the wall pressure amplitudes predicted theoretically for the case of $\theta = -45^\circ$. The theoretical solution qualitatively agrees with DNS. The quantitative discrepancy occurs because the receptivity model ignores the shock wave and its interaction with the incident acoustic wave. For $\theta = +45^\circ$ (radiating from above), the incident wave radiates over the total plate surface and contributes to the disturbance field in the boundary layer. In this case, the theory discussed herein is not valid because the theoretical solution does not contain the acoustic component in the far-downstream region. For this reason, the theoretical curves are not shown in figure 15(a, b).

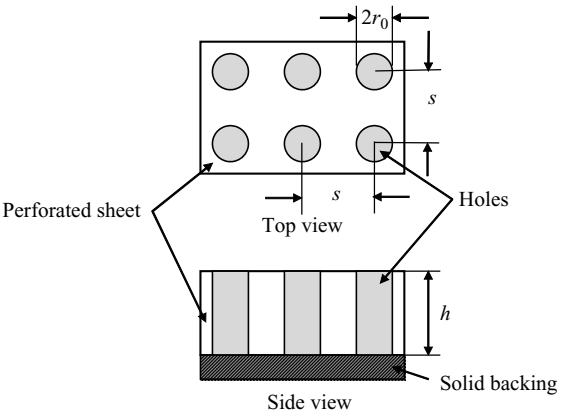

FIGURE 19. Porous coating of regular microstructure.

4. Disturbances over a porous coating

4.1. *Disturbances induced by suction-blowing*

For investigation of the boundary-layer stability, the initial disturbances are induced by the boundary condition modelling a local periodic suction-blowing near the leading edge (Egorov *et al.* 2006). The mass flow on the plate surface is given by

$$q_w(x,t) = \frac{\rho_w^* v_w^*}{\rho_\infty^* U_\infty^*} = \varepsilon \sin\left(2\pi \frac{x - x_1}{x_2 - x_1}\right) \sin(\omega t),\ x_1 \leqslant x \leqslant x_2,\ \ t > 0, \tag{3}$$

where ε is the forcing amplitude; $x_1 = 0.0358$, $x_2 = 0.0495$ are boundaries of the suction-blowing region and the circular frequency $\omega = 260$. The suction-blowing amplitude, $\varepsilon = 6 \times 10^{-4}$, was chosen small enough to compare numerical results with LST. For the unsteady problem, the wall temperature corresponds to the adiabatic wall temperature $T_w(x,t) = T_{ad}(x)$; i.e. the temperature disturbance is zero on the wall.

For modelling of the UAC effect, the boundary conditions on the porous wall are formulated using the analytical relation of Fedorov *et al.* (2001), which couples the vertical velocity disturbance with the pressure disturbance. In terms of real variables, this relation is written as

$$v_w(x,t) = p'_w(x,t)\mathrm{Re}(A_y) - \frac{1}{\omega}\frac{\partial}{\partial t}(p'_w(x,t))\mathrm{Im}(A_y). \tag{4}$$

where $p'_w(x,t) = p_w(x,t) - p_w(x,0)$, the pressure disturbance on the plate surface (difference between instant and steady-state pressure). In (4), the time derivative was approximated with the second order for the numerical integration. The UAC admittance, A_y, is expressed as

$$A_y = -n Z_0^{-1} \tanh(\Lambda h),$$

where n is porosity (ratio of the pore volume to the total volume of the coating); Z_0 and Λ are characteristic impedance and propagation constant for an isolated pore, and h is the porous layer thickness.

Herein, we consider a porous coating comprising equally spaced vertical cylindrical blind micro-holes (figure 19). The dimensionless pore radius is $r_0 = 0.333 \times 10^{-3}$, and $h = 5.5 \times 10^{-2}$. For this coating, Z_0 and Λ are calculated using the analytical relations derived by Fedorov *et al.* (2001). The boundary condition (4) is imposed in the region $x > 0.3$. Calculations are carried out for porosities $n = \pi/9$, $\pi/16$, which correspond

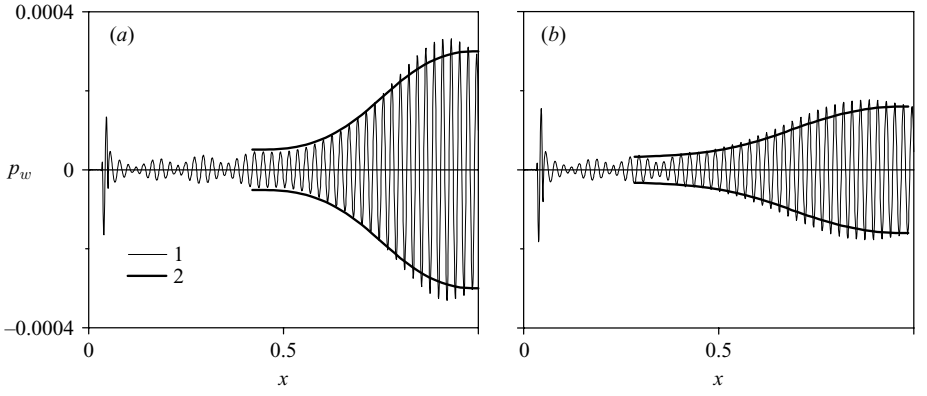

FIGURE 20. Pressure disturbances on (*a*) solid and (*b*) porous walls: 1, DNS; 2, LST.

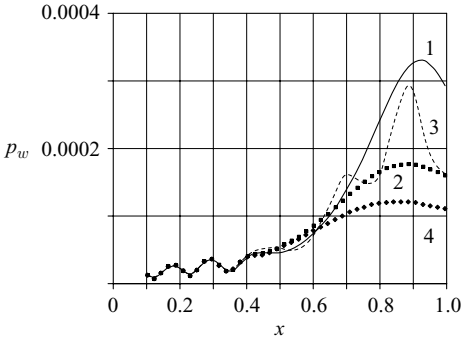

FIGURE 21. Amplitudes of wall-pressure disturbances: 1, solid; 2, porous wall of $n = \pi/16$; 3, piecewise porous wall of $n = \pi/16$; 4, porous wall of $n = \pi/9$.

to the pore spacing $s = 3r_0$ and $4r_0$, respectively. The UAC parameters are chosen so that the number of pores per disturbance wavelength is approximately 20 in the case of $s = 3r_0$ and 15 in the case of $s = 4r_0$ (the second-mode disturbance wavelength is $\lambda \approx 0.02$ for the considered frequency). It is assumed that the porous surface is aerodynamically smooth; i.e. the pore end effects are neglected.

In the case of $n = \pi/16$, the pressure-disturbance distributions along the solid (figure 20*a*) and porous (figure 20*b*) walls agree satisfactory with LST in the region where the second mode dominates. The porous coating leads to a significant decrease of the disturbance amplitude. In figure 21, the pressure-disturbance amplitude on the solid wall (curve 1) is compared with those on the porous wall of $n = \pi/16$ (curve 2) and $n = \pi/9$ (curve 4). Apparently, the UAC stabilization effect increases with porosity. In the region $x < 0.45$, which is upstream from the instability onset point, the UAC weakly affects the boundary-layer disturbances. The maximum effect is observed in the unstable region, where the coating suppresses the second-mode instability.

To estimate the UAC end effects associated with upstream and downstream junctures between solid and porous surfaces, we carried out calculations for a piecewise coating. The boundary condition (4), corresponding to the porous wall of $n = \pi/16$, is imposed in the strips: $0.3 < x < 0.4$, $0.5 < x < 0.6$, $0.7 < x < 0.8$ and $0.9 < x \leqslant 1$. The remaining surface part is solid (except for the narrow suction-blowing region).

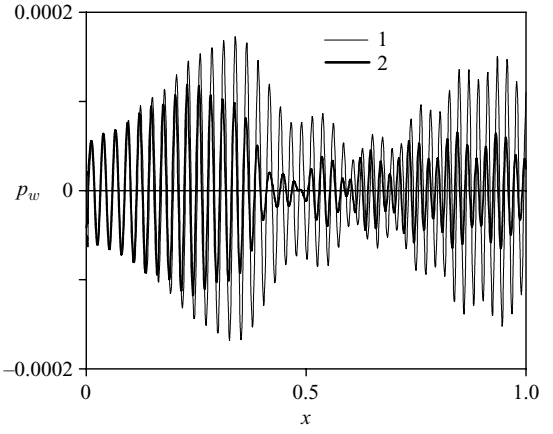

FIGURE 22. The wall pressure disturbance in the case of fast acoustic wave of zero angle of incidence: 1, solid wall; 2, porous wall of $n = \pi/16$.

In this case, the pressure-disturbance amplitude (curve 3 in figure 21) oscillates between curves 1 and 2 relevant to the solid and porous walls, respectively. The amplitude increases to the solid-wall level and decreases to the porous-wall level with approximately equal rate. The relaxation length in both directions is approximately $\Delta x_r \approx 0.05$ and corresponds to 2–3 wavelengths of the Mack second mode. This indicates that end effects are local and can be neglected in calculations of the integral UAC performance.

4.2. *Disturbances generated by acoustic waves*

To evaluate the UAC effect on the receptivity process, we impose the boundary condition (4) in the region $x > 0.1$. Calculations are performed for the coating of porosity $n = \pi/16$. Herein we consider fast and the slow acoustic wave of $\theta = 0^\circ$, and the fast acoustic wave of $\theta = +45^\circ$. The latter case was chosen to distinguish the UAC effect on acoustic disturbances. Since the fast acoustic wave of $\theta = +45^\circ$ is not synchronized with modes F and S, there is no appreciable excitation of unstable disturbances in the boundary layer. In all cases, the incident wave has amplitude $\varepsilon = 5 \times 10^{-5}$ and frequency $\omega = 260$.

The wall pressure disturbances are shown in figure 22 for the case of a fast acoustic wave of $\theta = 0^\circ$. Curve 1 corresponds to the solid wall, and curve 2 to the porous wall. The coating leads to a decrease of the mode F amplitude in the leading-edge region $0 < x < 0.4$. As a result, the disturbance amplitude in the region of inter-modal exchange ($0.6 < x < 0.7$) is noticeably lower than in the solid-wall case. In the unstable region $x > 0.7$, where mode S dominates, disturbances on the porous wall virtually do not amplify owing to the UAC stabilization effect. Note that the UAC slightly affects the disturbance phase speeds in the boundary layer and does not change the synchronization conditions. Comparison of the disturbance field patterns (not shown here) indicates that the UAC weakly affects the acoustic field.

Figure 23 shows the wall pressure disturbances for the case of a slow acoustic wave with $\theta = 0^\circ$. Curves 1 and 2 are relevant to the solid and porous walls, respectively. The LST and experiments (Fedorov *et al.* 2003*a*, *b*) show that the UAC stabilizes the Mack second mode and slightly destabilizes the first mode. Hence, mode S should be more unstable in the region $x < 0.6$ and more stable in the region $x > 0.7$. Exactly the same behaviour is predicted by DNS (see curves 1 and 2 in figure 23).

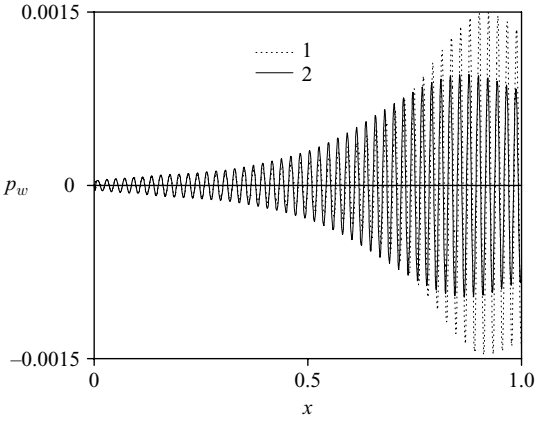

FIGURE 23. The wall pressure disturbance in the case of slow acoustic wave of zero angle of incidence: 1, solid wall; 2, porous wall of $n = \pi/16$.

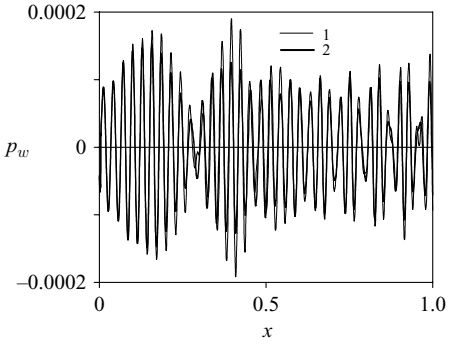

FIGURE 24. The wall pressure disturbance in the case of fast acoustic wave of $\theta = +45°$: 1, solid wall; 2, porous wall of $n = \pi/16$.

In the case of a fast acoustic wave with $\theta = +45°$, the phase speed predicted by DNS (figure 4, curve 4) remains approximately equal to the phase speed of the incident acoustic wave (figure 4, curves 1). This indicates that the acoustic wave is dominant in the boundary layer. Comparing the pressure disturbance distributions on the solid and porous walls (figure 24, curves 1 and 2), we conclude that the UAC weakly affects the near-wall acoustic field. Furthermore, in all cases, the DNS solution does not show appreciable excitation of the boundary-layer modes on the spatial non-uniformities associated with junctures between solid and porous surfaces. Seemingly, these detrimental effects are negligible.

5. Conclusions

Direct numerical simulation of receptivity to two-dimensional acoustic disturbances was carried out for the boundary-layer on a flat plate with sharp leading edge at the free-stream Mach number 6. Excitation of boundary layer modes by fast and slow acoustic waves of various angles of incidence was considered. Corresponding theoretical solutions were obtained using the leading-edge receptivity model of Fedorov & Khokhlov (1991, 1993, 2001) and the two-mode approximation (Fedorov 2003).

It was shown that the theoretical model captures basic features of the DNS solution. The quantitative discrepancy between theory and DNS is associated with the fact that the shock wave, which is formed near the plate leading edge owing to viscous–inviscid interaction, produces profound effect on the acoustic near field. This effect was not considered in the asymptotic theory of Fedorov & Khokhlov (1991, 1993, 2001) assuming that the shock wave is negligible. Near the plate leading edge, the shock layer behaves as a wedge-like waveguide, in which the disturbance field essentially depends on the angle of incidence θ and type of external acoustic waves. The slow wave radiating over the plate from above at $\theta = +45^\circ$ and the fast wave radiating over the plate from below at $\theta = -45^\circ$ weakly penetrate through the shock, and the shock layer is relatively quiet. On the contrary, the slow wave radiating over the plate from below ($\theta = -45^\circ$) and the fast wave radiating over the plate from above ($\theta = +45^\circ$) effectively excite waveguide modes.

Receptivity depends on both the level of acoustic near field and the difference between phase speeds of unstable boundary-layer waves and incident acoustic disturbances (synchronization condition). As this difference increases, the coupling between disturbances decreases in accordance with the theoretical model of Fedorov & Khokhlov (1991, 1993, 2001). An interplay between the synchronization detuning and the waveguide excitation leads to a non-monotonic dependency of the receptivity level on the angle of incidence θ. Receptivity to slow acoustic waves is higher than to fast waves. Note that slow acoustic waves are naturally radiated by vortices propagating in the turbulent boundary layer on walls of supersonic wind tunnels (Laufer 1964).

This numerical study demonstrates that even weak shocks may be important in the leading-edge receptivity process. The interaction of incident acoustic waves with the shock wave leads to the unexpected conclusion that, for the cases considered, the hypersonic flow over a flat plate is more receptive to slow acoustic waves radiating over the plate leading edge from below, than those radiating over the leading edge from above.

A porous coating of regular porosity (equally spaced cylindrical blind micro-holes) effectively diminishes the second-mode growth rate. In particular, the second-mode amplitude decreases twice on the surface covered by a UAC of 20% porosity. DNS results agree satisfactory with LST predictions for the second-mode disturbances. The UAC end effects, associated with junctures between solid and porous surfaces, were modelled for the case of piecewise porous coating. It was found that these effects are localized over $\sim$2–3 disturbance wavelengths and can be neglected in estimates of the integral UAC performance.

DNS modelling of the UAC effect on boundary-layer disturbances generated by free-stream acoustic waves was carried out. The porous coating essentially diminishes amplitudes of modes F and S, when the fast acoustic wave radiates over the flat plate at zero angle of incidence $\theta = 0^\circ$. A slow acoustic wave of $\theta = 0^\circ$ predominantly excites mode S. The UAC slightly destabilizes this mode in the upstream region (where mode S corresponds to the Mack first mode) and stabilizes it in the downstream region (where mode S corresponds to the Mack second mode). This is consistent with LST predictions.

A fast acoustic wave of $\theta = +45^\circ$ weakly excites the boundary-layer modes since it does not meet the synchronization condition. In this case, the acoustic field dominates in the boundary layer. DNS showed that the porous coating weakly affects the acoustic disturbances.

In summary, two-dimensional direct numerical simulation confirms the UAC stabilization concept for hypersonic flow over a flat plate. A two-dimensional

idealization is justified partially by the fact that the most unstable second-mode waves are two-dimensional. However, real noise sources and hypersonic configurations are three-dimensional. The nonlinear breakdown of unstable waves is associated with three-dimensional effects even in two-dimensional boundary layers. In our future work, three-dimensional DNS will be carried out to treat nonlinear effects as well as three-dimensional instabilities such as the first mode, cross-flow and Görtler vortices.

This work is supported by the Russian Foundation for Basic Research under Grant 06-08-01214 as well as the Air Force of Scientific Research under Contract FA9550-06-C-0097 monitored by Dr John Schmisseur.

REFERENCES

Balakumar, P., Zhao, H. & Atkins, H. 2002 Stability of hypersonic boundary-layer over a compression corner. *AIAA Paper* 2002-2848.

Bountin, D. A., Shiplyuk, A. N., Maslov, A. A. & Chokani, N. 2004 Nonlinear aspects of hypersonic boundary layer stability on a porous surface. *AIAA Paper* 2004-0255.

Demetriades, A. 1974 Hypersonic viscous flow over a slender cone, part III: Laminar instability and transition. *AIAA Paper* 74-535.

Djakov, S. P. 1957 Interaction of shocks with small disturbances. *Sov. Phys. J. Exp. Theor. Phys.* **33**, 948–961 (in Russian).

Egorov, I. V., Fedorov, A. V. & Nechaev, A. V. 2004 Receptivity of supersonic boundary layer on a blunt plate to acoustic disturbances. *AIAA Paper* 2004-249.

Egorov, I. V., Fedorov, A. V. & Soudakov, V. G. 2006 Direct numerical simulation of disturbances generated by periodic suction-blowing in a hypersonic boundary layer. *Theoret. Comput. Fluid Dyn.* **20**(1), 41–54.

Fedorov, A. V. 2003 Receptivity of a high-speed boundary layer to acoustic disturbances. *J. Fluid Mech.* **491**, 101–129.

Fedorov, A. V. & Khokhlov, A. P. 1991 Excitation of unstable modes in supersonic boundary layer by acoustic waves. *Fluid Dyn.* **9**, 456–467.

Fedorov, A. V. & Khokhlov, A. P. 1993 Excitation and evolution of unstable disturbances in supersonic boundary layer. In *Proc. ASME Fluid Engng Conf.* FED. **151**, 1–13.

Fedorov, A. V. & Khokhlov, A. P. 2001 Prehistory of instability in a hypersonic boundary layer. *Theoret. Comput. Fluid Dyn.* **14**(6), 359–375.

Fedorov, A. V., Malmuth, N. D., Rasheed, A. & Hornung, H. G. 2001 Stabilization of hypersonic boundary layers by porous coatings. *AIAA J.* **39**, 605–610.

Fedorov, A. V., Kozlov, V. F., Shiplyuk, A. N., Maslov, A. A., Sidorenko, A. A., Burov, E. V. & Malmuth, N. D. 2003*a* Stability of hypersonic boundary layer on porous wall with regular microstructure. *AIAA Paper* 2003-4147.

Fedorov, A. V., Shiplyuk, A. N., Maslov, A. A., Burov, E. V. & Malmuth, N. D. 2003*b* Stabilization of a hypersonic boundary layer using an ultrasonically absorptive coating. *J. Fluid Mech.* **479**, 99–124.

Forgoston, E. & Tumin, A. 2005 Initial-value problem for three-dimensional disturbances in a compressible boundary layer. *Phys. Fluids* **17**(8), 084106.

Gaponov, S. A. & Maslov A. A. 1980 *Disturbances Evolution in the Compressible Flows.* Nauka, Novosibirsk. (in Russian).

Guschin, V. R. & Fedorov, A. V. 1989 Short-wave instability in a perfect-gas shock layer. *Fluid Dyn.* **24**, 7–10.

Kendall, J. M. 1975 Wind tunnel experiments relating to supersonic and hypersonic boundary layer transition. *AIAA J.* **13**, 290–299.

Kimmel, R. 2003 Aspects of hypersonic boundary layer transition control. *AIAA Paper* 2003-0772.

Laufer, J. 1964 Some statistical properties of the pressure field radiated by a turbulent boundary layer. *Phys. Fluids* **7**(8), 1191–1197.

Ma, Y. & Zhong, X. 2001 Numerical simulation of receptivity and stability of nonequilibrium reacting hypersonic boundary layers. *AIAA Paper* 2001-0892.

Ma, Y. & Zhong, X. 2003*a* Receptivity of a supersonic boundary layer over a flat plate. Part 1. Wave structures and interactions. *J. Fluid. Mech.* **488**, 31–78.

Ma, Y. & Zhong, X. 2003*b* Receptivity of a supersonic boundary layer over a flat plate. Part 2. Receptivity to free-stream sound. *J. Fluid. Mech.* **488**, 79–121.

Mack, L. M. 1969 Boundary layer stability theory. Part B. Doc. 900-277. JPL, Pasadena, California.

Mack, L. M. 1975 Linear stability theory and the problem of supersonic boundary layer transition. *AIAA J.* **13**, 278–289.

McKenzie, J. F. & Westphal, K. O. 1968 Interaction of linear waves with oblique shock waves. *Phys. Fluids* **11**(11), 2350–2362.

Malik, M. R. 1989 Prediction and control of transition in supersonic and hypersonic boundary layers. *AIAA J.* **27**, 1487–1493.

Malik, M. R. 1997 Boundary-layer transition prediction toolkit. *AIAA Paper* 97-1904.

Malik, M. R., Zang, T. & Bushnell, D. 1990 Boundary layer transition in hypersonic flows. *AIAA Paper* 90-5232.

Malmuth, N. D., Fedorov, A. V., Shalaev, V. I., Cole, J., Khokhlov, A. P., Hites, M. & Williams, D. 1998 Problems in high speed flow prediction relevant to control. *AIAA Paper* 98-2695.

Maslov, A. A., Shiplyuk, A. N., Sidorenko, A. & Arnal, D. 2001 Leading-edge receptivity of a hypersonic boundary layer on a flat plate. *J. Fluid Mech.* **426**, 73–94.

Maslov, A., Shiplyuk, A., Sidorenko, A., Polivanov, P., Fedorov, A., Kozlov, V., & Malmuth, N. 2006 Hypersonic laminar flow control using a porous coating of random microstructure. *AIAA Paper* 2006-1112.

Morkovin, M. V. 1969 Critical evaluation of transition from laminar to turbulent shear layers with emphasis on hypersonic traveling bodies. *AFRL Rep* AFFDL-TR-68-149. Air Force Flight Dynamics Laboratory, Wright-Patterson AFB, OH, USA.

Rasheed, A., Hornung, H. G., Fedorov, A. V. & Malmuth, N. D. 2002 Experiments on passive hypervelocity boundary layer control using an ultrasonically absorptive surface. *AIAA J.* **40**, 481–489.

Reed, H. L., Kimmel, R., Schneider, S. & Arnal, D. 1997 Drag prediction and transition in hypersonic flow. *AIAA Paper* 97-1818.

Reshotko, E. 1976 Boundary-layer stability and transition. *Annu. Rev. Fluid Mech.* **8**, 311–349.

Stetson, K. F., Kimmel, R., Thompson, E. R., Donaldson, J. C. & Siler L. G. 1991 A comparison of a planar and conical boundary layer stability and transition at Mach number of 8. *AIAA Paper* 91-1639.

Zhong, X. 2001 Leading-edge receptivity to free-stream disturbance waves for hypersonic flow over parabola. *J. Fluid. Mech.* **441**, 315–367.